

# COOLING RATE CALCULATION AND MICROSTRUCTURE EVOLUTION OF Sm-Fe ALLOY POWDER PREPARED BY HIGH PRESSURE GAS ATOMIZATION

Received – Priljeno: 2022-08-24

Accepted – Prihvaćeno: 2022-12-20

Original Scientific Paper – Izvorni znanstveni rad

The  $\text{Sm}_2\text{Fe}_{17}$  alloy powder was prepared by high-pressure gas atomization technology, and its morphology and size distribution were analyzed. The relationship between the micro-structure evolution of the Sm-Fe alloy powder and the cooling rate was calculated. Besides, the relationship between the cooling rate of the high-pressure aerosolized alloy powder and the change of secondary dendrite arm spacing (SDAS) was verified. The cooling rate of the powder was indirectly determined according to the empirical relationship between the dendritic spacing of the rapidly solidified alloy and the cooling rate. After comparison, the results are consistent with the theoretical calculation.

*Keywords:* Sm-Fe alloy, powder prepared, cooling rate, SDAS, particle size, microstructure

## INTRODUCTION

$\text{Sm}_2\text{Fe}_{17}$  is the best material for the preparation of the fourth generation of rare earth permanent magnet SM-Fe-N alloy [1]. However, the low nitride rate has been restricting the acquisition of permanent magnet materials of Sm-Fe-N system with excellent performance [2]. Many scholars [3] have studied the atomization conditions of alloys, Parameters and the microscopic study of the powder, but the relationship between particle size, SDAS and cooling rate of Sm-Fe alloy powder prepared under the parameters has not been involved.

The purpose of this paper is to study the preparation and microstructure evolution of Sm-Fe alloy powder and the relationship between particle size, SDAS and cooling rate.

## EXPERIMENTATION

1 g of the powder was taken out for vacuum sealing and preservation, to be used for calculating the proportion of each size range. The number of powders in each size range and the relative proportion relationship were screened and counted as shown in Figure 1 and Figure 2. The remaining powders were screened using 900, 500, 360, 300, 200, 150 target screens, respectively, and preserved and marked in vacuum sealing, with different particle size ranges of <20  $\mu\text{m}$ , 20-30  $\mu\text{m}$ , 30-40  $\mu\text{m}$ , 40-50  $\mu\text{m}$ , 50-70  $\mu\text{m}$ , 70-100  $\mu\text{m}$  and >100  $\mu\text{m}$ .

Seven selected groups of powders were impregnated with epoxy resin cold mosaic, polished and etched with 4 % nitric acid alcohol for 20 s. After ensuring the

smoothness of the etched surface and the integrity of the secondary dendrite after simple observation by optical microscopy (OM), the secondary dendrite was photographed on the scanning electron microscopy (SEM) platform, and the OM and SEM observation images.

## RESULTS AND DISCUSSION

### Dimension distribution

The size of 2375 SM-Fe alloy powders was measured and statistically analyzed by Image-Pro Plus 6.0. Figure 1 is a cross-sectional topography diagram of a single particle in seven size ranges. Figure 2 plots seven groups of size range particle size relative proportion curve and generally presents a normal distribution, in which that proportion of powders with particle size less than 50  $\mu\text{m}$  is 79,75 %, and the overall distribution is uniform and small.

### Microscopic observation

As shown in Figure 3(a, b), because of the low cooling rate, the powder particles grow into coarse dendrite

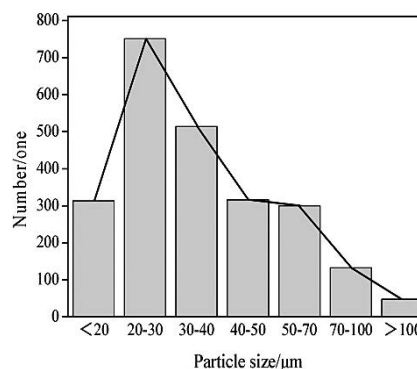


Figure 1 Number of powders in each dimension range

J.W. Liu (E-mail: 1968653452@qq.com), C.Y. Song, Y.L. Gui, S.W.Chen, S.H. Wang. Metallurgy and Energy College, North China University of Science and Technology, Tangshan, China. Tangshan Key Laboratory of Special Metallurgy and Material Manufacture, Tangshan, China

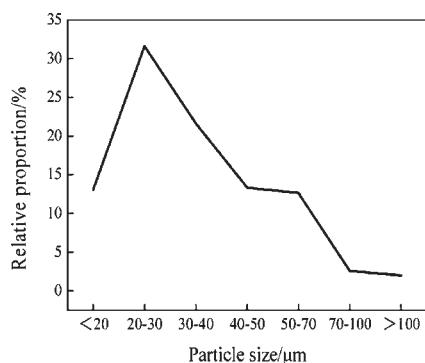


Figure 2 Relative proportion of powder in each size range

with the composition of  $\alpha$ -Fe during solidification, and the diameter of the primary dendrite can reach 2 ~ 3  $\mu\text{m}$ , and the secondary dendrite arm spacing can reach 1,203  $\mu\text{m}$ . With the increase of cooling rate, the coarse dendrite becomes finer from the outer edge to the center, and the secondary dendrite arm spacing decreases in Figure 3(c) ~ (e). Observe Figure 3(f) ~ (h), as the particle size of the powder further decreases, the dendrites gradually refined are improved in macroscopic distribution, and finally grow into fine equiaxed dendrites.

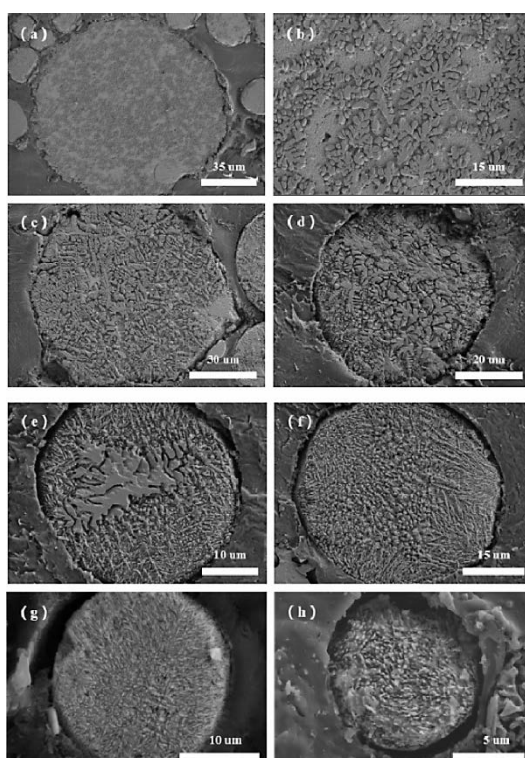


Figure 3 Eight size range particle surface topography: (a) > 100  $\mu\text{m}$  (b) 75-100  $\mu\text{m}$  (c) 50-75  $\mu\text{m}$  (d) 40-50  $\mu\text{m}$  (e) 30-40  $\mu\text{m}$  (f) 20-30  $\mu\text{m}$  (g)  $\leq 20 \mu\text{m}$  (h)  $\leq 10 \mu\text{m}$

### Measurement of SDAS

Figure 4 randomly selects a schematic diagram of a specific method of particle SDAS measurement. When using the special measurement tool Image-Pro Plus 6.0, it is necessary to select six SDAS in each particle (the

yellow cross line is belonging to a dendrite, each of which is measured three times (the three pairs of red parallel lines on the right side are three times, and each pair of parallel lines is measured three times separately) and at least ten different particles were selected for measurement, each group was measured 180 times, and the seven groups totaled 1 260 times. The seven groups of powders were measured separately and the corresponding SDAS data were counted. As shown in Figure 5, for the sake of simplicity, only the relative cumulative frequency curves of SDAS in a range of sizes [4,5].

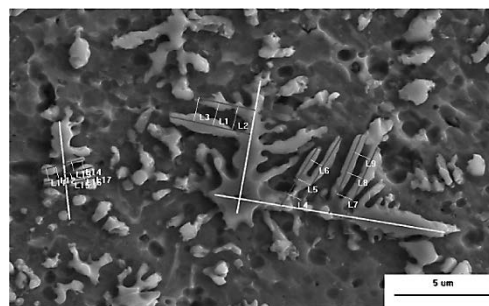


Figure 4 Schematic diagram of measurement

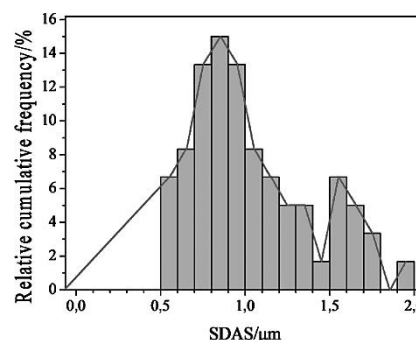


Figure 5 Relative cumulative frequency of SDAS measured between 75  $\mu\text{m}$  and 106  $\mu\text{m}$

The average SDAS corresponding to the seven groups of powders of different size ranges were calculated and plotted as a function of particle size in Table 1. As shown in Figure 6, according to the lattice diagram, the relationship between SDAS and particle size of Sm-Fe alloy powder with particle size less than 100  $\mu\text{m}$  can be roughly deduced as follows:

$$D = 0,01d + 0,2 \tag{1}$$

Where  $D$  stands for SDAS/  $\mu\text{m}$ ,  $d$  stands for the particle size of the powder/  $\mu\text{m}$ .

After a total of 5040 SDAS measurements were carried out for the other four different atomization parameters, and finally the relationship between SDAS and particle size satisfies the above function curves. It can be inferred that there is a direct relationship between particle size, cooling rate and SDAS, that is, the particle size increases with the increase of SDAS, which means that the cooling rate is slower. Therefore, the specific cooling rate of each Sm-Fe alloy powder can be judged by particle size or SDAS.

Table 1 Average SDAS for powders in each dimension range

Particle size range/ $\mu\text{m}$	SDAS / $\mu\text{m}$
$D > 100$	1,203
$75 < D \leq 100$	1,036
$50 < D \leq 75$	0,813
$40 < D \leq 50$	0,615
$30 < D \leq 40$	0,522
$20 < D \leq 30$	0,410
$D \leq 20$	0,296

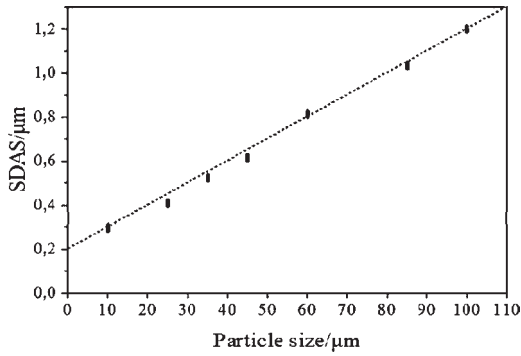


Figure 6 Schematic diagram of average SDAS as a function of size

### Conversion to cooling rate

From the experimental process of high-pressure atomization of samarium iron powder, it can be seen that the heat transfer of atomized melt droplets mainly depends on the release of heat from the interface to the surrounding environment, and the cooling mode follows Newton heat transfer mode. Zhou Peter et al [6] summed up the heat balance condition of melt droplets in flight as follows: the heat released by the droplets equals to the heat flux transferred from the droplets surface to the ambient atmosphere, and obtained the empirical formula of the droplet cooling rate:

$$\varepsilon = -\frac{6h}{\rho C_p d} (T_d - T_f) \tag{2}$$

Where  $\varepsilon$  represents the cooling rate/ $\text{K}\cdot\text{s}^{-1}$  represents the density of molten metal droplet/ $\text{kg}\cdot\text{m}^{-3}$ .  $C_p$  represents the equivalent specific heat capacity of the droplets/ $\text{J}\cdot(\text{kg}\cdot\text{K})^{-1}$ .  $d$  represents powder particle size/ $\mu\text{m}$ .  $T_d$  represents the temperature before droplet atomization/ $^{\circ}\text{C}$ .  $T_f$  represents the ambient temperature is also the chamber temperature/ $^{\circ}\text{C}$ .  $h$  represents the convective heat transfer coefficient, specifically to the mathematical form can be described as:

$$h = \frac{2k_g}{d} + 0,6k_g \sqrt{\frac{U\rho_g}{\mu_g d}} \tag{3}$$

Where  $k_g$  represents the thermal conductivity of the ambient gas/ $\text{W}\cdot(\text{m}\cdot\text{K})^{-1}$  represents the flow rate of the ambient gas relative to the droplet/ $\text{m}\cdot\text{s}^{-1}$ .  $\rho_g$  represents the ambient gas Density/ $\text{kg}\cdot\text{m}^{-3}$ .  $\mu_g$  represents the dynamic viscosity of the ambient gas/ $\text{N}\cdot\text{s}\cdot\text{m}^{-2}$ .

In this experiment, the ambient gas, that is, the atomizing gas is high-purity argon. The thermal physical parameters are shown in Table 2 [7-9].

Table 2 Thermophysical parameters of high purity argon

$k_g/(\text{W}\cdot(\text{m}\cdot\text{K})^{-1})$	$\rho_g/(\text{kg}\cdot\text{m}^{-3})$	$\mu_g/(\text{N}\cdot\text{s}\cdot\text{m}^{-2})$
0,018	1,784	$2,250 \times 10^{-5}$

Substituting the above table data into the formula (2) paralleling the formula (1) to derive the formula for calculating the cooling rate of the molten droplets of the alloy, namely:

$$\varepsilon = \frac{6}{\rho C_p} (T_d - T_f) \left( \frac{0,036}{d^2} + 3,04 \sqrt{\frac{U}{d^3}} \right) \tag{4}$$

The specific parameter values involved in the atomization experiment are shown in Table 3 [10].

Table 3 Cooling rate calculations involving parameters

$\rho / \text{kg}\cdot\text{m}^{-3}$	7 740
$C_p / \text{J}\cdot(\text{kg}\cdot\text{K})^{-1}$	398
$T_d / ^{\circ}\text{C}$	1 620
$T_f / ^{\circ}\text{C}$	30
$U / \text{m}\cdot\text{s}^{-1}$	400
$d / \mu\text{m}$	10 ~ 200

The experimental process parameters were substituted into the formula, and the cooling rate of the powder particles having a particle diameter of  $10 \mu\text{m} \sim 200 \mu\text{m}$  was calculated. The results are shown in Figure 7. The cooling rate of the atomized Sm-Fe alloy powder is between  $6,94 \times 10^4 \text{K}\cdot\text{s}^{-1}$  to  $7,08 \times 10^6 \text{K}\cdot\text{s}^{-1}$ , and the cooling rate decreases with decreasing particle size. When the particle size does not exceed  $30 \mu\text{m}$ , the cooling rate can reach the order of  $10^6 \text{K}\cdot\text{s}^{-1}$  or more, which is  $1,27 \times 10^6 \text{K}\cdot\text{s}^{-1}$ . When the particle diameter is less than  $20 \mu\text{m}$ , the cooling rate sharply increases. When the particle size is larger than  $50 \mu\text{m}$ , the cooling rate changes slightly and gradually becomes mild. When the particle size is  $170 \mu\text{m}$ , the cooling rate is reduced to  $10^4 \text{K}\cdot\text{s}^{-1}$ .

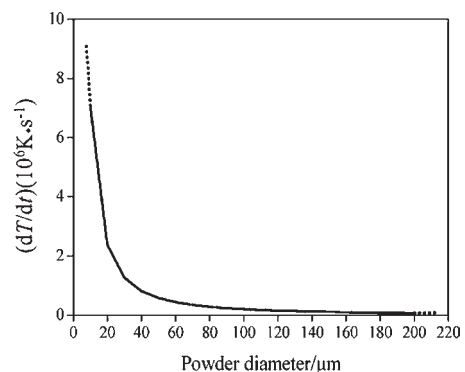


Figure 7 Relationship between cooling rate of droplets and particle size

## Transformation relationship between SDAS and cooling rate

That is, the equation of SDAS and cooling rate for atomized samarium ferroalloy powder is derived by combining the relationship between SDAS and particle size and the empirical formula between cooling rate and particle size derived above:

$$\left( \frac{3,6 \times 10^{-6}}{(D-0,2)^2} + \frac{3,04 \times 10^{-3}}{(D-0,2)} \sqrt{\frac{U}{D-0,2}} \right) \quad (5)$$

Bring each data into the above equation and plot the relationship between SDAS and cooling rate, as shown in Figure 8. With the increase of SDAS, the cooling rate decreases and when SDAS increases to 0,7  $\mu\text{m}$ , the change relationship tends to be mild. When SDAS is less than 0,4  $\mu\text{m}$ , the cooling rate begins to increase sharply. The experimentally obtained atomized powder has SDAS of 0,3~0,5  $\mu\text{m}$  occupies the most, the cooling rate is faster and the order of magnitude is above  $10^6 \text{K}\cdot\text{s}^{-1}$ .

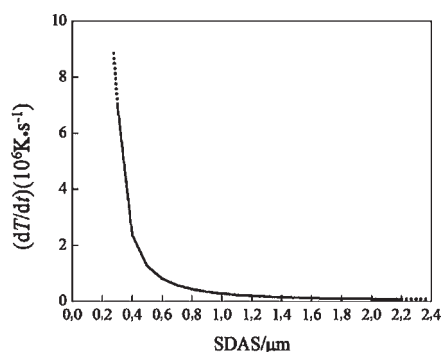


**Figure 8** Relationship between cooling rate of droplets and SDAS

## Verification of the relationship between powder SDAS and cooling rate

In order to verify the relationship between the high-pressure atomized bismuth iron alloy powder SDAS and the cooling rate derived above, it is usually verified using an empirical formula. The empirical formula is:

$$\lambda = B(\varepsilon)^n \quad (6)$$

Where  $B$  and  $n$  are constants, for Sm-Fe alloys,  $\lambda$  is dendritic spacing/  $\mu\text{m}$ .

The average SDAS of the seven sets of size range powders was substituted into the empirical formula to plot the relationship between SDAS and cooling rate, as shown in Figure 7. At the same time, compared with Figure 8, the final verification result is basically consistent with the derivation calculation result.

## CONCLUSIONS

The powder with a particle size below 50  $\mu\text{m}$  accounts for about 79,75 %, and the overall distribution is uniform and small. With the decreasing of the particle size and the increasing of the cooling rate, the surface of the powder becomes smoother and smoother. At the same time, the coarse dendritic crystals are improved in the macroscopic distribution, and finally grow into fine equiaxed dendritic structure. The cooling rate of the powder prepared by the experiment is between  $6,94 \times 10^{-4} \text{K}\cdot\text{s}^{-1}$  to  $7,08 \times 10^6 \text{K}\cdot\text{s}^{-1}$  and the cooling rate increases with the decrease of droplet size.

As the SDAS increases, the cooling rate decreases and when SDAS increases to 0,7  $\mu\text{m}$ , the change relationship tends to be mild. When the SDAS is less than 0,4  $\mu\text{m}$ , the cooling rate sharply increases. The SDAS of the atomized powder obtained in the experiment occupied the most at 0,3  $\mu\text{m}$  ~ 0,5  $\mu\text{m}$ , and the cooling rate was faster and the order of magnitude was above  $10^6 \text{K}\cdot\text{s}^{-1}$ .

## Acknowledgments

Presented research was supported by Hebei Natural Science Funds for Distinguished Young Scholar (E2019209473)

## REFERENCES

- [1] W. X. Wu, Y. Q. Guo, A. H. Li, W. Li, *Acta Physica Sinica*. 57(2008)4.
- [2] J. M. D. Coey, H. Sun, *Journal of Magnetism and Magnetic Materials*. 87 (1990)251.
- [3] B. B. Lv, D. B. Yu, S. R. Zhang, Y. Luo, *Journal of Rare Earths*. 31 (2013) 979.
- [4] Y. A. Ma, Y. W. Xin, *Foreign Metal Materials*. 3 (1989)35.
- [5] S. L. Liang, T. Liu, K. Li, *China Foundry*. 2 (2016)107.
- [6] B. D. Zhou, Z. D. Xie, J. Shen, *Materials Science and Technology*. 1 (2001)79.
- [7] Y. X. Dai, M. Yang, C. J. Song, Q. J. Zhai, *Casting Technology*. 30 (2009)496.
- [8] M. C. Han, P. T. Ni, Y. Shu, Y. M. Zhang, C. C. Wang, Y. J. Dong, J. C. Yang, *Rare Metals Materials and Engineering*. 37 (2008)655.
- [9] J. G. Zhang, H. S. Shi, D. S. Sun, *Journal of Materials Processing Technology*. 138 (2003)357.
- [10] A. Inoue, Masumoyot, T Ekimoyot, *Metallurgical Transactions A*. 19 (1988)235.

**Note:** The responsible for English language is J. W. Liu.